Magnetic Proximity Effect and Superconducting Triplet Correlations at the Heterostructure of Cuprate Superconductor and Oxide Spin Valve

K. Y. Constantinian, G. A. Ovsyannikov, V. V. Demidov and Yu. N. Khaydukov

Abstract We report on studies of heterostructure made of a cuprate superconductor $YBa_2Cu_3O_{7-d}$, a ruthenate/manganite ($SrRuO_3/La_{0.7}Sr_{0.3}MnO_3$) spin valve, and thin gold film (Au). It is shown that a magnetic moment is excited in the cuprate superconductor due to magnetic proximity effect, at the same time magnetic moment is suppressed in the ruthenate/manganite part. The measurements showed that magnetic moment penetration depth significantly exceeds the coherence length of the cuprate superconductor. The induced magnetic moment could be attributed to coupling of the Cu and Mn atoms by a covalent chemical bond resulting in a strong hybridization and orbital reconstruction. The mesa-structures with micrometer sizes were prepared by adding superconducting niobium film (Nb) adjacent to the gold, forming a second superconducting electrode. The DC superconducting current flowing across the mesa-structure was observed even in the case when interlayer thicknesses were much greater than the coherence lengths of the ferromagnets in heterostructure. The maximum of the critical current took place when the thicknesses of ferromagnetic films in spin valve were near to the coherence lengths of the ferromagnets. Obtained data agree with the theoretical predictions for occurrence of the spin-triplet pairing. We measured superconducting current when applied magnetic field was by two orders

K. Y. Constantinian (✉) · G. A. Ovsyannikov · V. V. Demidov
Kotelnikov Institute of Radio Engineering and Electronics RAS, Mokhovaya 11, bld.7, Moscow 125009, Russia
e-mail: karen@hitech.cplire.ru

G. A. Ovsyannikov
e-mail: gena@hitech.cplire.ru

V. V. Demidov
e-mail: demidov@cplire.ru

Yu. N. Khaydukov
Max-Planck Institute for Solid State Research, 70569 Stuttgart, Germany
e-mail: Yury.Khaydukov@frm2.tum.de

A. Sidorenko (ed.), *Functional Nanostructures and Metamaterials for Superconducting Spintronics*, NanoScience and Technology,
https://doi.org/10.1007/978-3-319-90481-8_4

greater than the field level required for one magnetic flux quantum nucleation in the mesa-structure. Although theory for long-range spin-triplet pairing predicts a dominance of the second harmonic, our estimation of the second harmonic amplitude in the current-phase relation of superconducting current did not exceed 50% of the first one.

1 Introduction

In a contact of a superconductor (S) with a normal (non-superconducting) metal (N), superconducting correlations penetrate at the distance which is much grater than the interatomic one [1]. This phenomenon is known as a proximity effect, and first was discussed in detail by de Gennes [2, 3]. Along with the penetration of superconducting correlations into the normal metal, there is a change in superconducting order parameter due to a "leakage of Cooper pairs" at the interface. Earlier it was assumed that due to the "antagonism" between superconductivity and magnetism, there is no proximity effect at the superconductor (S) and ferromagnet (F) interface. Larkin and Ovchinnikov [4], and Fulde and Ferrell [5] predicted an occurrence of inhomogeneous superconducting correlations (LOFF state) in an S/F structure. The presence of LOFF states in the junction was manifest by oscillations of the superconducting critical current with temperature and F-interlayer thickness [6, 7].

In 2001, it was theoretically demonstrated that the triplet superconducting correlations (TSC) with nonzero spin projection together with the usual (singlet) one at the S/F interface occur [8, 9]. A distinctive feature of TSC is the fact that they are insensitive to the exchange field and penetrate into the ferromagnet at distances that are typical for a non-magnetic metal. Experimentally the occurrence of TSC was recorded by the presence of a superconducting current in structures composed of two superconductors with singlet superconductivity coupled by a ferromagnetic interlayer with spiral magnetization [10] as well as for ferromagnetic film with non-uniform magnetization [11]. TSCs in superconducting structures with a ferromagnetic interlayer made of two ferromagnets ($S/F_L/F_R/S$) were theoretically predicted for ballistic electron transport [12] and for diffuse scattering [13]. It was theoretically demonstrated that a second harmonic in the current-phase relation (CPR) of a superconducting current dominates [10, 12–14].

In oxide structures such as a cuprate superconductor–manganite ferromagnet, the transparency of the interface is determined by a work function and can be low [15]. It limits the proximity effect. The reports about the excitation of triplet correlations at the cuprate superconductor and manganite ferromagnet interface are rather contradictory [16–21]. It should be noted that the manganites $La_{0.7}Sr_{0.3}MnO_3$ (LSMO) and $La_{0.7}Ca_{0.3}MnO_3$ (LCMO) used in the experiment are ferromagnets having 100% carrier polarization (magnetic half-metal) at low temperatures. The appearance of singlet excitations at the ferromagnet boundary is suppressed that does not exclude the excitation of spin-triplet correlations.

The ferromagnetic correlations from the ferromagnet at F/N interface penetrate into the N-metal at a small interatomic distance due to the locality of the exchange interaction [22, 23]. It was theoretically demonstrated that at the S/F interface, there is a change in the density of states due to its difference for electrons with spin-up and spin-down ones [24–27]. The sign and magnitude of the magnetic moment occurring in the superconductor strongly depend on the parameters of the S/F interface, such as transparency, impurities, and layer thickness [28–31]. An experimental study of the magnetic proximity effect in S/F structures based on ferromagnets and metal superconductors that was performed using a variety of methods (ferromagnetic resonance, muon scattering, neutron scattering, etc.) generally confirmed the conclusions of the theory [32–35].

The presence of a magnetic moment in cuprate superconductor in $YBa_2Cu_3O_7/La_{2/3}Ca_{1/3}MnO_3]_n$ ($[YBCO/LCMO]_n$) superlattices was revealed [36–40]. An induced magnetic moment of the Cu atoms oriented antiparallel to the magnetic moment of Mn atoms was detected at interface using X-ray dichroism technique [38–40]. It was shown that the Cu and Mn atoms were connected through the interface by a covalent chemical bond, resulting in a strong hybridization and orbital reconstruction. The typical lengths of the orbital reconstruction greatly exceed the interatomic distances and are equal to 8–10 nm [41, 42].

Here we present results on experimental investigation of the changes of magnetic moment in the heterostructure containing the cuprate superconductor and ferromagnetic spin valve. Measurements of the heterostructure's magnetic moment were carried out by SQUID magnetometer and ferromagnetic resonance (FMR) technique. Analysis of data obtained allowed us to determine the magnitude of the magnetic moment induced in the superconductor, as well as the change of magnetic moment in the ferromagnetic spin valve.

Then the results of experimental studies of superconducting and quasiparticle currents in micrometer size mesa-structures Nb/Au/LSMO/SRO/YBCO with a top electrode made of Nb are presented as well. We evaluated characteristic parameters, such as the depth of the penetration of superconducting correlations into a ferromagnet and the transparency of the cuprate superconductor–ruthenate ferromagnet interface. The contribution of the second harmonic of the superconducting current-phase relation was experimentally determined. Based on the experimental data, we concluded that the contribution of the triplet superconducting correlations to the transport of superconducting carriers in mesa-structures is dominant.

2 Experimental

We studied epitaxial thin-film heterostructures consisting of a cuprate superconductor $YBa_2Cu_3O_{7-\delta}$ and two ferromagnetic layers $SrRuO_3$ (SRO) and $La_{0.7}Sr_{0.3}MnO_3$ prepared by laser ablation at temperatures of 700–800 ºC and oxygen pressure of 0.3–0.6 mbar. The thickness of the superconductor was in the range of 80–200 nm, whereas the thickness of the ferromagnetic layers varied from 5 to 20 nm (see Table 1).

Table 1 Composition and thickness of the test heterostructures, as well as the experimentally determined changes of magnetic moment of the heterostructures. d_S is the thickness of the YBCO film, d_{SRO} is the thickness of the SRO film, d_{LSMO} is the thickness of the LSMO film, and Δm is the change of magnetic moment

N	Substrate	d_S, nm	d_{SRO}, nm	d_{LSMO}, nm	Δm, 10^{-6} emu
1	(001)$LaAlO_3$	80	20	14	10
2	(110)$NdGaO_3$	80	17	7	(5 ± 1.5)
3	(110)$NdGaO_3$	180	0	20	$\leq(1 \pm 2)$
4	(001)LSAT	150	13	25	2.5
5	(110)$NdGaO_3$	0	14	40	–
6	(110)$NdGaO_3$	0	0	50	–

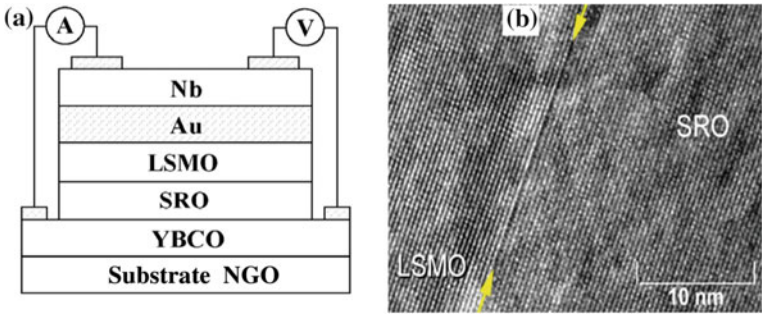

Fig. 1 **a** Cross section of a mesa-structure and the measurement circuit, **b** an image of the interface between SRO and LSMO, obtained by transmission electron microscope JEM-2100 with the 8×10^5 zoom. The interface is marked by arrows

The heterostructures were covered by thin (20 nm) layer of gold on top. We used substrates with the dimensions 5×5 mm made of (110)$NdGaO_3$ (NGO). The magnetization vector of the LSMO film deposited on a (110)NGO substrate (or YBCO film) is generally lays in the plane of the substrate [43, 44] whereas for SRO film is outside of the plane of the substrates used [45]. LSMO with a uniaxial magnetic anisotropy of 20–30 mT at the room temperature and exchange energy of 2.3 meV [49] and SRO with a magnetic anisotropy of about 1 T and exchange energy of 13 meV [50] were used. The surface properties were tested for film satellites on an atomic-force microscope, and fairly sharp boundaries between the SRO/LSMO layers were observed by transmission electron microscope (Fig. 1b).

We investigated mesa-structures with an Au-Nb bilayer served as the top superconducting electrode. The bilayer was deposited by magnetron sputtering [43].

3 Magnetic Proximity Effect

Magnetic moment in heterostructures. A detailed study of the field and temperature dependences of magnetization in the separate films and heterostructures was conducted using a SQUID magnetometer MPMS-3 [46]. The plane of the substrate was set relative to the direction of the magnetic field within 1°–2°. Table 1 shows used substrate and thicknesses of the heterostructure films, as well as the changes of the magnetic moments of the heterostructure, Δm.

The values of Δm for samples N2 and N3 are obtained from FMR measurements and correspond to the changes in magnetization of the SRO layer for heterostructures No. 2 and the LSMO film for heterostructure No.3; the rest of the measurements were carried out for changes in magnetization of the entire structure. In the sample No. 4, we used a $(LaAlO_3)_{0.3}(Sr_2AlTaO_6)_{0.7}$ (LSAT) substrate, onto which we deposited the epitaxial film made out of a calcium-doped cuprate superconductor $Y_{0.7}Ca_{0.3}Ba_2Cu_3O_x$.

Figure 2 shows a family of temperature dependences for the magnetic moment parallel to the substrate plane $m_{\|}$, for heterostructure No. 1. These dependences are obtained using the SQUID magnetometer during cooling in a magnetic field (FC mode). The external magnetic field was located in the substrate plane and was directed along one of its edges. Detailed measurements of the magnetic anisotropy have shown that the substrate edges form an angle of 40º–50º relative to the easy axis of the LSMO magnetic anisotropy. For the temperatures $T<T_{SRO}$ (the Curie temperature of the SRO film $T_{SRO} \approx 150$ K for the given heterostructure), $m_{\|}$ is determined by the sum of the LSMO film magnetic moment and the projections of the SRO film magnetic moment on the direction of the magnetic field. Under the influence of a magnetic field magnetic moment, $m_{\|}$ changes due to the rotation of the LSMO and SRO film magnetic moments. As a result, magnetic moments of LSMO and SRO films give smaller total magnetic moment of the spin valve at low fields than that of the LSMO film at the same temperature, whereas at $H > 1$ kOe it is larger. The results of measuring the field dependence of magnetic moment m of the Au/LSMO/SRO/YBCO heterostructure (see No. 1 in Table 1) are shown in the inset of Fig. 2a for a magnetic field directed along the substrate edge at the temperature $T = 100$ K, which is higher than the critical temperature of the superconductor (T_C). The position of the magnetization easy axis of the SRO film is close to the normal to the substrate plane. The non-collinearity of the magnetization vectors of the ferromagnetic films contributes to the generation of superconducting triplet correlations having a nonzero spin projection of superconducting carriers, in the ferromagnetic interlayer [43, 49, 50].

At $T \approx T_C$ when magnetic field is parallel to the substrate plane, there is a sharp increase in the magnetic moment of the heterostructure (Fig. 2a). The thickness of the YBCO film $d_S = 80$ nm is less than the London penetration depth of the magnetic field. The magnetic field that is directed along the plane of the film completely penetrates the superconductor, and the diamagnetic response is not observed as expected due to the Meissner effect.

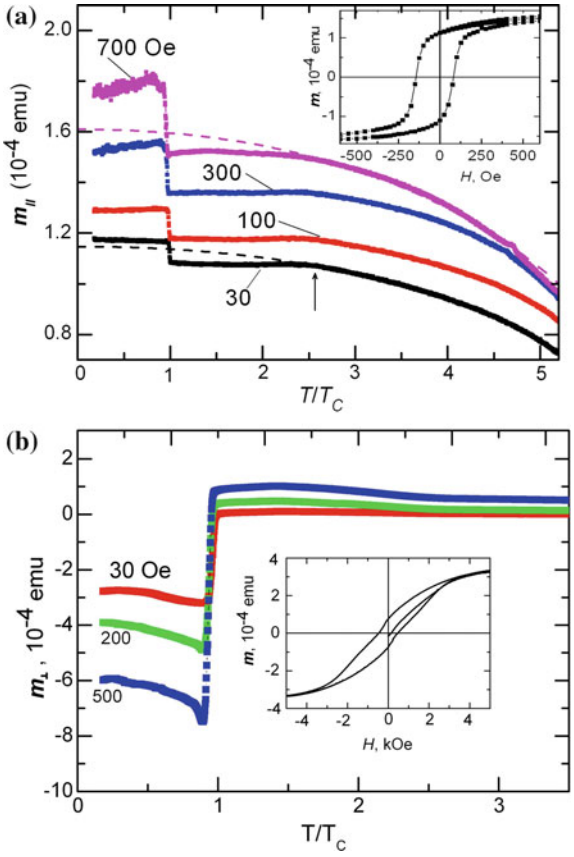

Fig. 2 Temperature dependences of magnetic moment of Au/LSMO/SRO/YBCO heterostructure in FC mode, 1 kOe, for magnetic field directed in parallel to the substrate plane (**a**) and in perpendicular (**b**). The transition of SRO to ferromagnetic state is observed at $T/T_C = 2.5$. Insets show the hysteresis loops for the corresponding magnetic field direction

The occurrence of a magnetic moment in a cuprate superconductor contacting manganite was theoretically considered in [42]. It was demonstrated that as a result of the antiferromagnetic interaction of the spins $x^2 - y^2$ of Cu electrons with e.g. electrons of Mn, an induced negative spin polarization in the cuprate superconductor occurs. The impact of this process on the properties of the superconductor is much stronger than injecting the spin-polarized electrons of the ferromagnet. It was determined this mechanism is responsible for induced magnetic moment in the $[YBCO/LCMO]_n$ superlattice [17]. The magnetic moment of the Cu atom induced in the superconductor is equal to 0.23 μ_B/Cu and is directed against the magnetic moment of Mn. Assuming that the change in the magnetic moment of our heterostructure occurs due to copper atoms located in a 10 nm thick layer, we obtain $\Delta m \sim 10^{-5}$ emu in sample No. 1 (see Fig. 2a) and the induced magnetic moment

~0.25 μ_B/Cu. The change to the direction of the copper magnetic moment in the YBCO/SRO contacts, observed both in [51] and in our case, can be caused by the negative magnetization of the SRO film [27, 45].

If the magnetic field is directed perpendicularly to the plane of the superconducting film, then the shielding currents occur in the layer $\lambda_\perp = \lambda_L^2/d_S \approx 0.3$ μm on the edge of the film. The magnetic field gets pushed out of the superconducting film and a diamagnetic response is observed (Meissner effect). This can be seen on the dependence of the magnetic moment $m_\perp(T)$ of the heterostructure, measured in the direction of the magnetic field that is perpendicular to the plane of the substrate (see Fig. 2b). It is easy to determine the superconductor critical temperature T_C in the heterostructure using the dependence $m_\perp(T)$. Note that the form of the dependences of perpendicular $m_\perp(T)$ does not change if we change measurement modes (FC or ZFC).

Ferromagnetic resonance in the heterostructure. The heterostructures were also studied using a Bruker ER 200 magnetic resonance spectrometer, operating in the frequency $\omega/2\pi = 9.7$ GHz. We measured ferromagnetic resonance spectra over a wide range of temperatures: 20–300 K. The FMR spectra of the LSMO film in the heterostructures were obtained by cooling the sample in the field of the Earth. Upon reaching the given temperature, we scanned the magnetic field from 0 to 4 kOe. The FMR spectrum from the SRO film does not measured at our experimental conditions due to the large value of the magnetic anisotropy field of the SRO film.

During the measurement of the ferromagnetic resonance spectrum, the magnetic component of the microwave field was perpendicular to the plane of the substrate. The external magnetic field H was always located in the plane of the substrate (parallel orientation) whereas in experiments with sample cooling, it was put along the magnetization easy axis of the induced uniaxial anisotropy of the LSMO film. The direction of this axis was predetermined from the angular dependences of the resonance field H_{CF}, taken at different temperatures under the conditions of magnetic field rotations around the normal to the substrate plane in a parallel orientation [44]. The angular dependences of the FMR spectrum of thin ferromagnetic film in the presence of uniaxial and biaxial anisotropy are described by the following equation [44]:

$$\left(\frac{\omega}{\gamma}\right)^2 = (H_0 + H_u \cos 2\varphi_u + H_c \cos 4\varphi_c)\left(4\pi M_0 + H_0 + H_u \cos^2 \varphi_u + H_c \frac{1 + \cos^2 2\varphi_c}{2}\right) \quad (1)$$

wherein γ is the gyromagnetic ratio, $H_u = 2K_u/M_0$, $H_c = 2K_c/M_0$, K_u and K_c are uniaxial anisotropy and cubic anisotropy constants correspondingly, the M_0 parameter is equal to the equilibrium magnetization in the absence of adjacent ferromagnetic layers, and φ_u and φ_c are angles at which the uniaxial and cubic anisotropy easy axes of magnetization are directed, relative to the external magnetic field, respectively. As a result of fitting the experimental data (Fig. 3) using (1), we were able to determine the following ferromagnetic parameters: K_u, K_c, M_0, as well as the direction of both the uniaxial and cubic anisotropy easy axes (see inset in Fig. 3). As noted previously, the processing of the angular dependences of the FMR spectra according

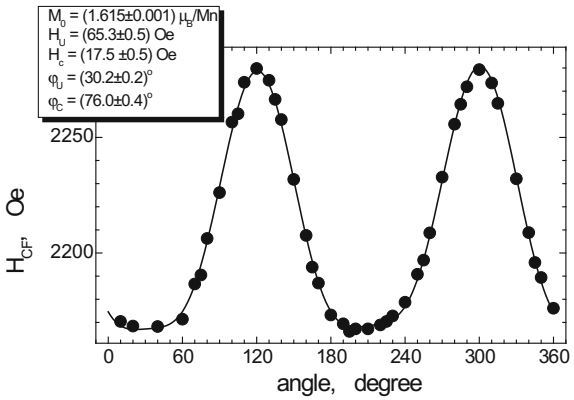

Fig. 3 Angular dependence of the resonant magnetic field at T = 295 K, heterostructure Au/LSMO/SRO/YBCO. The solid line was obtained using (1) with fitting parameters shown in the inset

to (1) allows us to determine the M_0 parameter and the directions of the easy axes in the LSMO films of the heterostructures.

The interlayer exchange between two ferromagnets must be considered at lower temperatures, because it leads to a resonance relation that differs from the (1). The temperature dependences of FMR spectra of the LSMO film in the heterostructure No. 2 have been measured. At $T \leq T_C$, when the YBCO film is in the superconducting state, a huge signal of non-resonant absorption was recorded at low magnetic fields having a hysteresis in the magnetic field. As a result, the FMR signals were recorded with an increase in the error of resonant field H_{CF} at $T < T_C$, but allow us to determine the superconducting transition temperature T_C of YBCO films. At $T > T_C$, the values of H_{CF} are determined much more accurately.

Figure 4 shows the temperature dependences of the resonant field H_{CF} for FMR signals from LSMO films in Au/LSMO/SRO/YBCO (N5) and Au/LSMO/YBCO (N6) heterostructures in vicinity of T_C of superconducting films. In all cases, the external magnetic field was directed along the easy magnetization axis. It is evident that for the Au/LSMO/SRO/YBCO heterostructure, there is a sharp change in the resonant field in the superconducting transition range.

Since in the Au/LSMO/SRO/YBCO heterostructure the LSMO film is separated from the superconducting YBCO film by the ferromagnetic SRO film, the jump of the resonance field H_{CF} of the LSMO layer could be associated with the change in magnetization of the SRO film. So, one must take into account the interlayer exchange interaction between LSMO and SRO which occurs through the magnetically ordered boundary layer with a high conductivity [52–55]. Using the procedure outlined in [56, 57], we obtained an expression that describes the relationship between the frequency and the resonance field for the LSMO layer in the LSMO/SRO heterostructure. The expression is similar to (1) but its value for the resonant field should be replaced with this combination

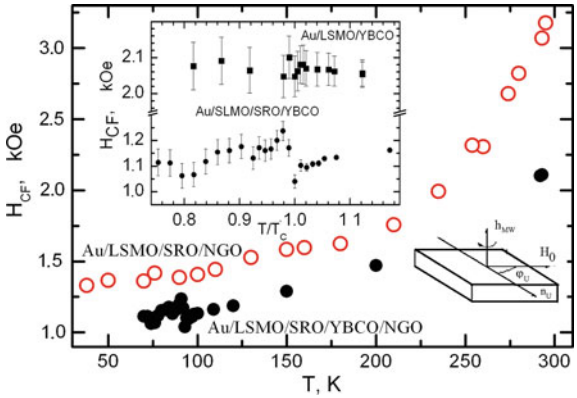

Fig. 4 Temperature dependence of the resonance field in the LSMO film for two heterostructures: Au/LSMO/YBCO and Au/LSMO/SRO/YBCO. The top inset shows the temperature dependence of the resonance field of these heterostructures in the vicinity of T_C. The bottom inset shows the geometry of FMR spectrum measurements

$$H_{CF} + \frac{H_{J1}^{\mathrm{LSMO}}\left(H_{CF} + H_{J1}^{\mathrm{SRO}}\right)}{H_{\mathrm{SRO}} - 4\pi M_{\mathrm{SRO}} - H_{J2}^{\mathrm{SRO}}}. \tag{2}$$

Here H_{SRO} and M_{SRO} represent the field of the uniaxial magnetic anisotropy and the magnetization of the SRO film correspondingly, $H_{J1}^{\mathrm{LSMO,SRO}}$ and H_{J2}^{SRO} are the effective fields of bilinear and biquadratic interlayer exchanges, respectively. For the corresponding layers, the magnitudes of these fields are inversely proportional to the magnetization of the corresponding layers [56, 57]. In order to fulfill the resonance ratio, it is required that the combination in (2) was constant on both sides of the magnetization jump. It allows us to obtain the relation between the changes of the resonant field δH_{CF} in the LMSO film and the magnetization of the SRO film δH_{CF}:

$$\frac{\delta M_{\mathrm{SRO}}}{M_{\mathrm{SRO}}} \approx \frac{\delta H_{CF}}{H_{CF}} \frac{H_{\mathrm{SRO}}}{4\pi M_{\mathrm{SRO}}} \tag{3}$$

An assessment of δH_{CF} performed in accordance with (3) shows that change in magnetization of the SRO film during the YBCO transition to the superconducting state is about ~$0.5M_{\mathrm{SRO}}$. Taking into account the contribution of the SRO film (m_{SRO} ~ 10^{-5} emu) to the total magnetic moment $m\|$ of the heterostructure (Fig. 2a), we find that the change of magnetic moment of the composite ferromagnet is smaller than the magnetic moment induced in the superconductor. Note that the positive sign of δM_{SRO} indicates that the magnetization of the SRO film decreases, since in this layer the magnetization has a negative sign (see also [27]). According to Fig. 4, we can also see that in the Au/LSMO/YBCO heterostructure, in which the ferromagnetic LSMO film is in contact with the YBCO film, a remarkable change in the magnetization of LSMO at $T \approx T_C$ is not detected. This difference in the

Au/LSMO/YBCO heterostructure can be explained by the absence of excitation of the triplet component of the superconducting current in the ferromagnetic interlayer [22, 27, 49, 50, 58] and low transparency of the YBCO/LSMO interface [50]. This leads to a negligibly small penetration of the superconducting order parameter from YBCO into the LSMO film and therefore, to a negligibly small change in the magnetic moment of the LSMO film in the heterostructure.

4 Superconducting Triplet Correlations

Electron transport in mesa-structures. Micrometer-sized mesa-structures in which the two superconductors YBCO and the Au-Nb bilayer are separated by a magnetic spin-valve SRO/SLMO were used. Five square-shaped mesa-structures with linear dimensions in the plane L = 0, 20, 30, 40, and 50 μm were prepared on a substrate (hereinafter referred to as "chip") using ion beam etching, and photolithography. A SiO_2 film with a thickness of 40 nm was used to isolate the contact at the edges of the mesa-structure. The scheme of measurements and the cross section of the mesa-structure are shown in Fig. 1a. The resistive characteristics of the satellite film and current–voltage characteristics (I-V curve) of mesa-structures were measured using four-point probe (see Fig. 1a) over the temperature range 4.2 K < T < 300 K, magnetic fields H of up to 2 kOe, and microwave monochromatic signal at frequencies f_e = 1–3 GHz and 36–45 GHz. Microwaves at frequency band of 1–3 GHz were applied to the sample by a coaxial cable. To reduce the influence of external electromagnetic fields, the measurements were conducted in a shielded box with filter on leads in. By varying the thickness of the interlayer, it was possible to estimate the penetration depth of superconducting correlations into the ferromagnetic layer.

On temperature dependence of mesa-structure resistance *R(T)* (Fig. 5), there are two highlighted regions of resistance reduction which correspond to the transition of YBCO and Au-Nb bilayer films to the superconducting state correspondingly. Above the critical temperature YBCO T_C the dependence $R(T)$ has a linear metal-type dependence, which is typical for the temperature dependence of a YBCO electrode. At $T < T_C$, the value of R decreases rapidly while features of interlayer ferromagnetic films are not observed. This behavior is explained by the fact that below the critical temperature of YBCO, the contribution from LSMO and SRO films into the value $R_N A$ (area $A = L^2$) is inferior to the contribution from the interface resistance of mesa-structure. Additional measurements showed that the resistance of Au-Nb bilayer film in normal state is also small [59]. As a result, in the temperature range $T < T_C$ the resistance of the mesa-structure is combined with the resistance of the interfaces between the boundaries between materials YBCO/SRO, SRO/LSMO, LSMO/Au:

$$R_{\mathrm{MS}} = R_{\mathrm{YBCO/SRO}} + R_{\mathrm{SRO/LSMO}} + R_{\mathrm{LSMO/Au}}.$$

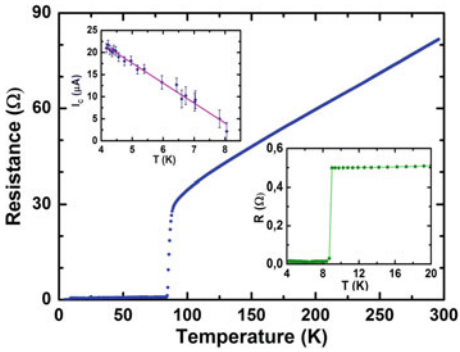

Fig. 5 Temperature dependence of the mesa-structure resistance $R(T)$. The bottom inset shows an enlarged area of $R(T)$ at low temperatures, whereas the top inset shows the temperature dependence of the critical current

In order to clarify the contribution from each of the interfaces that define the resistance of the composite layer mesa-structure, we also prepared mesa-structures with a single ferromagnetic interlayer. For mesa-structures with an SRO interlayer, the value $R_N A$ is almost three orders of magnitude lower than for a structure with an LSMO interlayer. If we assume that the resistance of the LSMO/Au border does not exceed the value of 1 $\mu\Omega$ cm^2 [60], then the resistance of the YBCO/LSMO/Au mesa-structure (100 $\mu\Omega$ cm^2) can be explained by the dominance of the YBCO/LSMO interface resistance. Using the data from [60], we find that the resistance of the SRO/Au interface can be estimated to be 0.05 $\mu\Omega$ cm^2, whereas the resistance of the YBCO/SRO border is about 0.1 $\mu\Omega$ cm^2, which is consistent with the data in [61]. Consequently, the value of $R_N A$ of the mesa-structure is determined mainly by the sum of the resistances of $R_{\mathrm{LSMO/Au}}$ and $R_{\mathrm{YBCO/SRO}}$ [50].

The critical current of a mesa-structure. Superconducting current was observed for the most of the mesa-structures under investigation having interlayer thickness up to 50 nm. The critical current I_C decreases linearly as the temperature increases (inset in Fig. 5) over the temperatures $4.2\mathrm{K} < T < T_C^{Au-Nb}$. For comparison, in mesa-structures with one ferromagnetic interlayer (LSMO or SRO), the superconducting current is absent at interlayer thicknesses exceeding 5 nm, which is about equal to the coherence length ξ_F. At smaller interlayer thicknesses, the superconducting current found on some samples was caused by pinholes. The presence of a critical current decline for the spin-valve thicknesses greater than 5 nm is an indication of the spin-triplet superconducting correlation transport via the spin valve [13, 62].

Outlines of the experimental values for the critical current density j_C for LSMO and SRO film thicknesses between 0 and 20 nm are shown in Fig. 6. We can see a peak for critical current density at layer thicknesses $d_{\mathrm{LSMO}} \approx 6$ nm and $d_{\mathrm{SRO}} \approx 8$ nm. Note that the critical current maximum in superconducting structures with a two-layer composite ferromagnetic interlayer is predicted at thicknesses that are about equal to the coherence length [63]. Since the mean free path l in oxide materials

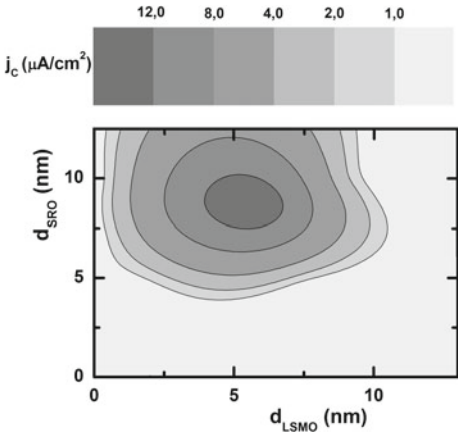

Fig. 6 Outlined regions of critical current density as a function of the plane thickness of spin-valve ferromagnetic layers at $T = 4.2$ K

(SRO and LSMO) is sufficiently small [64, 65], we can assume that the electron transport is diffusive in nature.

Magnetic field dependences. For the Josephson junction with a uniform critical current distribution, the critical current as the function of the magnetic field is described by the Fraunhofer relationship

$$I_C(H) = I_C(0)\left|\frac{\sin(\pi\Phi/\Phi_0)}{\pi\Phi/\Phi_0}\right| \tag{4}$$

where $\Phi_0 = 2.06783461 \times 10^{-15}$ Wb is the magnetic flux quantum and $\Phi = \mu_0 H S_{eff}$ is the magnetic flux of the external field in the mesa-structure [66, 67]. The zeros of the Fraunhofer dependence are observed when the external field through a cross section of the mesa-structure is equal to the magnetic flux quantum $\Phi \approx \Phi_0$. The measured magnetic field dependences of critical currents of mesa-structures were markedly different from the (4). Changing the direction of the magnetic field sweep (from ascending to descending, and vice versa), a hysteresis is observed caused by ferromagnetic nature of the interlayer materials [43]. Moreover, the critical current was observed at considerably high levels of magnetic field up to 2 kOe (see Fig. 7a). Therefore, at $H = 1.3$ kOe the value $I_C = 16.5$ μA which composes 94% of the $I_C(H = 0)$ and 0.7 of the maximum measured at $H = -6.5$ Oe. Note that in YBCO/Au/Nb structures without magnetic interlayer [68] or with an antiferromagnetic $Ca_{0.7}Sr_{0.3}CuO_2$ interlayer [69], the critical current dropped sharply with an increasing of magnetic field. While it even increased in the mesa-structures at fields greater than 1 kOe. This unusual behavior of the critical current in the structures with a metallic ferromagnetic interlayer was mentioned also in [70].

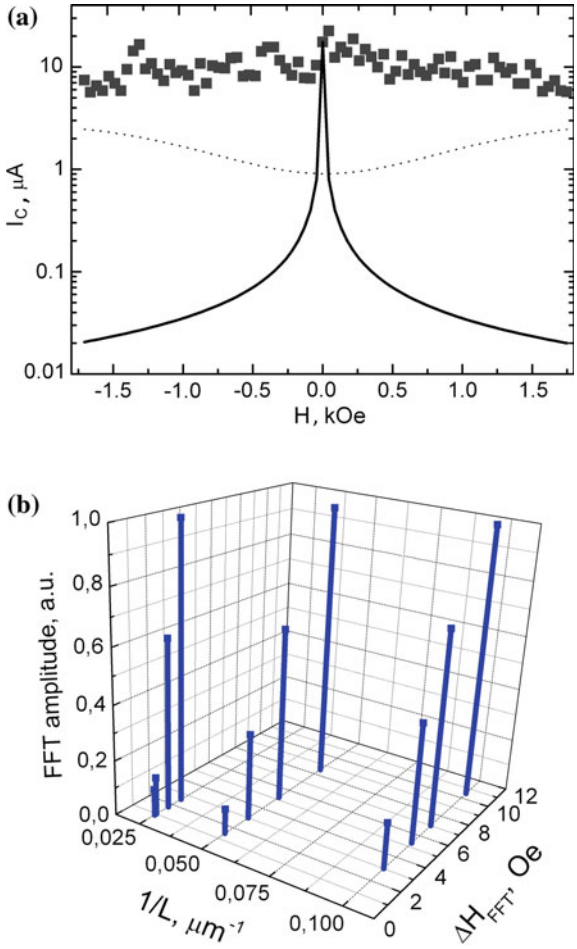

Fig. 7 Dependence of the critical current on the magnetic field over a wide range of magnetic fields for the mesa-structure with $d_{\mathrm{SRO}} = 8.5$ nm, $d_{\mathrm{LSMO}} = 3$ nm, $L = 10$ μm. The solid line shows the expected decline of the maxima of the values I_C of the Fraunhofer oscillatory dependence (4). The dotted line shows the level of noise that limits our ability to measure the critical current (**a**). The periods ΔH_{FFT} and amplitudes of the Fourier components as a function of parameter $1/L$ for magneto-field dependences of the critical current of three mesa-structures with $L = 10, 20, 40$ μm, arranged on a chip (**b**)

There are several mechanisms that determine the critical current versus magnetic field dependence as follows: the penetration of the magnetic flux quanta (Josephson vortices) which creates the "Fraunhofer" oscillation, the emergence of a domain structure in the ferromagnetic interlayer, and the rotation of the layer magnetization under the influence of external magnetic field. Note that in the absence of triplet correlation, the superconducting current according to (4) must be significantly sup-

pressed in the magnetic field at $\Phi \gg \Phi_0$. Several quanta of magnetic flux penetrate into the transition since the maxima of the Fraunhofer dependence fall at a rate of $1/\Phi$ (see Fig. 7a).

In assessing the effective area of penetration of the magnetic field directed along the plane of the transition $S_{\text{eff}} = Ld'$, the magnetic permeability of the layers must be taken into account $d' = \mu_1 d_{\text{LSMO}} + \mu_2 d_{\text{SRO}} + \lambda_{\text{Nb}} + \lambda_{\text{YBCO}}$ where $\lambda_{Nb} = 90$ nm and $\lambda_{\text{YBCO}} = 150$ nm are the London penetration depths of the magnetic field for Nb and YBCO, respectively, and $\mu_{1,2}$ is the magnetic permeability for the spin valve. For the Josephson junctions with the ferromagnetic interlayer, the effective thickness increases by $\mu = 1 + \chi$ times [67, 71] where χ is the magnetic susceptibility. The values $\mu_1 = 12$, $\mu = 3$ were obtained from the magnetic field dependences of the spin-valve interlayer magnetic moment of a mesa-structure with $d_{\text{LSMO}} = 6$ nm and $d_{\text{SRO}} = 8.5$ nm and $L = 10$ nm. Substituting these values of the critical current minima for the mesa-structure should be located at $\Delta H = 6$ Oe due to the penetration of the Josephson vortices. This value is slightly different from the experimental value of $\Delta H \approx 10$ Oe which is the distance between the minima for $I_C(H)$. During the calculation of χ, we used data from the measurement of the magnetic moment $M(H)$ for a direction of the external magnetic filed coinciding with the hard axis [49]. Fourier analysis of the oscillatory dependences $I_C(H)$ for three mesa-structures with the identical thickness d' shows the presence of at least two periods ΔH_{FFT} with significant FFT amplitudes (see Fig. 7b). At the same time, there is an increase in ΔH_{FFT} proportional to $1/L$. It is known that the domain structure in the ferromagnetic interlayer could have a dramatic effect on the electron transport mechanism [72, 73]. The domain generated non-uniformities of magnetization in the LSMO films could lead to an additional modulations of the $I_C(H)$ dependences. However, based on the data in Fig. 7b we can see that the oscillations $I_C(H)$ are not caused by the domain structure. The effective area of the magnetic field penetration $S_{\text{eff}} = d_{\text{dom}} d'$ must correspond to much greater periods of critical current oscillations due to magnetic field, than the values ΔH_{FFT} in the figure. The presence of the Fourier transform components with fractional periods ΔH_{FFT} is most likely indicative of superconducting current-phase relation (CPR) deviation from the sinusoidal form [49, 50].

Microwave dynamics of mesa-structures. A study of the high-frequency dynamics of Shapiro steps on the I-V curve when microwave radiation is applied proves the absence of pinholes ("short-circuiting") between superconducting electrodes. This is confirmed by the presence of Shapiro step oscillations in response to microwave power. The amplitudes of steps are in good agreement with the resistively shunted junction model (RSJ) [59]. The absence of pinholes is ensured by thick interlayers. The roughness of the layers is smaller than the thickness of LSMO and SRO films. A comparison of the experimental Shapiro steps with those calculated according to the modified RSJ model [59] allows us to determine the CPR of superconducting current. Measurements of CPR were carried out in a zero magnetic field and during cooling the mesa-structures in a constant magnetic field (100–200 Oe). A family of I-V curves obtained under microwave radiation at frequency of 41 GHz is shown in Fig. 8a. Since the frequency of the microwave signal f_e is greater than the characteristic frequency of the mesa-structure $f_e >> f_C = \frac{2e}{h} I_C R_N$, McCumber

parameter $\beta_C = \frac{2\pi}{\Phi_0} I_C R_N^2 C << 1$ the impact of capacitance of the mesa-structure could be ignored. Under these conditions, the appearance of fractional Shapiro steps on the I-V curve (see Fig. 8a) clearly points on non-sinusoidal nature of the CPR [59]. Figure 8b shows the experimental and theoretical dependences of the critical current I_C and the first Shapiro step I_1 versus normalized microwave current $x = I_{RF}/I_C\omega$ where I_{RF} is the amplitude of the microwave current and $\omega = f_e/f_C$. The ratio of the amplitude of the second harmonic in CPR to the first one $q = I_{C2}/I_{C1}$ was determined according to the numerical approximation of the critical current and Shapiro step amplitudes as functions of the microwave power [49, 50]. Due to the influence of the second harmonic in CPR, the critical current and the first Shapiro step have nonzero local minima (see Fig. 8b). Since it was assumed that $I_{C1} \approx I_C$ (valid for $q < 1$), then the values of q determined by this method are underestimated. According to the theoretical study in [13] during the excitation of spin-triplet correlations in the junction with bilayer interlayer, the second harmonic dominates in CPR increasing with the disorientation angle of interlayer magnetization reaching a maximum at angles close to $\pi/2$. According to the measurements obtained using the SQUID magnetometer at low fields, the magnetization projection of the SRO film is directed in the direction opposite to the magnetization of LSMO that determines the magnetization direction angle for the LSMO film. At fields greater than the values of the anisotropy field (200–300 Oe), the magnetization of the LSMO layer is directed along the field. Therefore, we should observe the growth of the second harmonic in CPR in small fields. However, in the microwave experiment on five mesa-structures, we did not observe an increase of the second harmonic in range of magnetic fields 20–50 Oe as predicted in [12–14] and the ratio of amplitude of second harmonic to the critical current did not exceed the value of $q = 0.5$.

5 Conclusion

The manifestation of an induced magnetic moment in the superconductor is experimentally observed in the heterostructure based on the cuprate superconductor with the ferromagnetic spin valve. The magnetic moment occurring in the superconductor coincides with the calculations for the magnetic moment of Cu atoms induced due to the orbital reconstruction at the S/F interface. The typical penetration depth of the magnetic moment into the superconductor is significantly greater than the coherence length of the cuprate superconductor. It is experimentally shown that in superconducting mesa-structures with the spin valve LSMO/SRO interlayer, the superconducting current is observed when the total layer thickness is up to 50 nm. This thickness of the interlayer is significantly greater than the coherence length. The maximum value of the critical current density is observed at interlayer thicknesses that are close to the coherence length of the ferromagnetic films. The oscillations of periods of magnetic field critical current dependence arise due to the deviation of the superconducting current-phase relation from the sinusoidal form. This feature is confirmed by microwave measurements of the Shapiro step heights as functions of

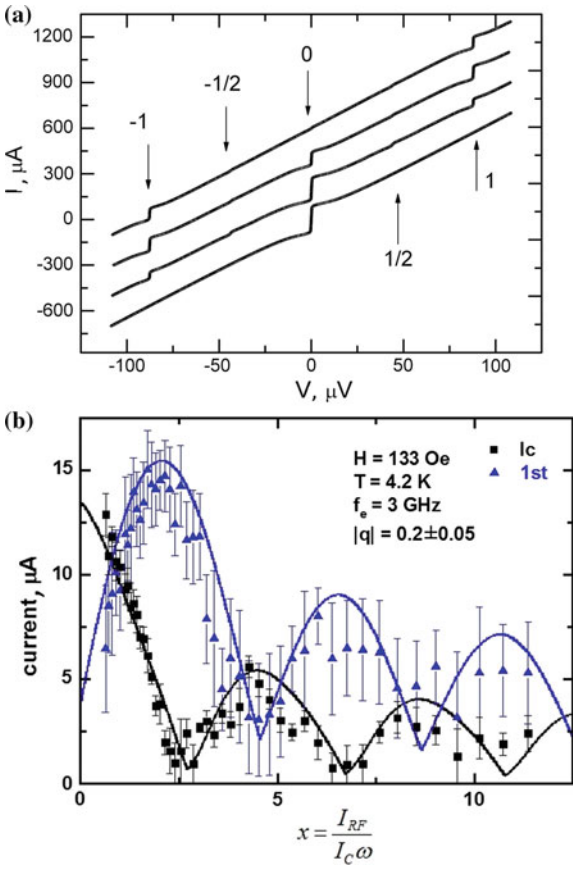

Fig. 8 A set of I-V curves for the mesa-structure with d_{SRO} = 8.5 nm, d_{LSMO} = 6 nm, L = 10 μm when subjected to electromagnetic radiation with a frequency fe=41 GHz. The arrows indicate the number n of the Shapiro steps on the voltage axis, n = 0 corresponds to the critical current I_C (**a**). The dependence of the critical current amplitude and the first Shapiro step for the mesa-structure with d_{SRO} = 5.6 nm, d_{LSMO} = 15 nm, L = 50 μm, f_e = 3 GHz (**b**)

applied microwave power. The large value of the second harmonic in CPR up to 50% of the critical current was evaluated. Another factor which may affect magnetic field dependence of the critical current is the impact of magnetic domains in the interlayer.

Acknowledgements The authors wish to thank V.A. Atsarkin, I.V. Borisenko, A.F. Volkov, A.V. Zaitsev, B. Keimer, A.I. Kalabukhov, Yu.V. Kislinskiy, G. Logvenov, A.M. Petrzihk, A.V. Shadrin, A.E. Sheyerman, and D. Winkler for their assistance in conducting these experiments and the useful discussions.

References

1. A.I. Buzdin, Rev. Mod. Phys. **77** (2005)
2. G. Deutscher, P.G. de Gennes, Proximity effects, in *Superconductivity*, ed. by R.D. Parks (Dekker, NewYork, 1969), pp. 1005–1034
3. P.G. de Gennes, Phys. Lett. **23**, 10–11 (1966)

4. A.I. Larkin, Yu.N. Ovchinnikov, JETP **47**, 1136 (1964)
5. P. Fulde, R. Ferrell, Phys. Rev. **135**, A550 (1964)
6. A.I. Buzdin, L.N. Bulayevskiy, S.V. Panyukov, JETP Lett. **35**, 147 (1982)
7. V.V. Ryazanov, V.A. Oboznov, AYu. Rusanov, A.V. Veretennikov, A.A. Golubov, J. Aarts, Phys. Rev. Lett. **86**, 2427 (2001)
8. F.S. Bergeret, A.F. Volkov, K.B. Efetov, Phys. Rev. Lett. **86**, 4096 (2001)
9. A. Kadigrobov, R.I. Shekhter, M. Jonson, Europhys. Lett. **54**, 394 (2001)
10. J.W.A. Robinson, J.D.S. Witt, M.G. Blamire, Science **329**, 59 (2010)
11. M.S. Anwar, F. Czeschka, M. Hesselberth, M. Porcu, J. Aarts, Phys. Rev. B **82**, 100501 (2010)
12. L. Trifunovic, Z. Popovíc, Z. Radovíc, Phys. Rev. B **84**, 064511 (2011)
13. C. Richard, M. Houzet, J.S. Meyer, Phys. Rev. Lett. **110**, 217004 (2013)
14. L. Trifunovic, Phys. Rev. Lett. **107**, 047001 (2011)
15. S. Yunoki, A. Moreo, E. Dagotto, S. Okamoto, S.S. Kancharla, Phys. Rev. B **76**, 064532 (2007)
16. C. Visani, Z. Sefrioui, J. Tornos et al., Nat. Phys. **2318**, 1 (2012)
17. T. Hu, H. Xiao, C. Visani, Z. Sefrioui, J. Santamaria, C.C. Almasan, Phys. Rev. B **80**, 060506R (2009)
18. Y. Kalcheim, T. Kirzhner, G. Koren, O. Millo, Phys. Rev. B **83**, 064510 (2011)
19. T. Golod, A. Rydh, V.M. Krasnov, I. Marozau, M.A. Uribe-Laverde, D.K. Satapathy, Th. Wagner, C. Bernhard, Phys. Rev. B **87**, 134520 (2013)
20. M. van Zalk, A. Brinkman, J. Aarts, H. Hilgenkamp, Phys. Rev. B **82**, 134513 (2010)
21. A.M. Petrzhik, G.A. Ovsyannikov, A.V. Shadrin, K.Y. Constantinian, A.V. Zaitsev, V.V. Demidov, Yu.V. Kislinskiy, JETP **139**, 1190 (2011)
22. H. Zabel, S. D. Bader (eds.), *Magnetic Heterostructures, Advances and Perspectives in Spinstructures and Spintransport*. Springer Tracts in Modern Physics, vol. 227 (Springer, Berlin, Heidelberg, 2008), pp. 251–289
23. W.L. Lim, N. Ebrahim-Zadeh, J.C. Owens et al., Appl. Phys. Let. **102**, 162404 (2013)
24. K. Halterman, O.T. Valls, Phys. Rev. B **66**, 224516 (2002)
25. R. Fazio, C. Lucheroni, Europhys. Lett. **45**, 707 (1999)
26. V.N. Krivoruchko, E.A. Koshina, Phys. Rev. B **66**, 0145621 (2002)
27. F.S. Bergeret, A.F. Volkov, K.B. Efetov, Phys. Rev. B **69**, 174504 (2004)
28. F.S. Bergeret, A.L. Yeyati, A. Martin-Rodero, Phys. Rev. B **72**, 064524 (2005)
29. M.Yu. Kharitonov, A.F. Volkov, K.B. Efetov, Phys. Rev. B **73**, 054511 (2006)
30. R. Grein, T. Löfwander, M. Eschrig, Phys. Rev. **88**, 054502 (2013)
31. M. Alidoust, K. Halterman, J. Linder, Phys. Rev. B **89**, 054508 (2014)
32. I.A. Garifullin, D.A. Tikhonov, N.N. Garif'yanov, et al., Appl. Magn. Reson. **22**, 439 (2002)
33. M.G. Flokstra, S.J. Ray, S.J. Lister et al., Phys. Rev. B. **89**, 054510 (2014)
34. J. Xia, V. Shelukhin, M. Karpovski et al., Phys. Rev. Lett. **102**, 087004 (2009)
35. R.I. Salikhov, I.A. Garifullin, N.N. Garif'yanov, et al., Phys. Rev. Lett. **102**, 087003 (2009)
36. J. Stahn, J. Chakhalian, Ch. Niedermayer, et al., Phys. Rev. B **71**, 1405098 (R) (2005)
37. D.K. Satapathy, M.A. Uribe-Laverde, I. Marozau et al., Phys. Rev. Lett. **108**, 197201 (2012)
38. J. Chakhalian, J.W. Freeland, G. Srajer et al., Nat. Phys. **2**, 244 (2006)
39. J. Chakhalian, J.W. Freeland, H.-U. Habermeier et al., Science **318**, 1114 (2007)
40. H.-U. Habermeier, J. Phys.: Conf. Ser. **108**, 012039 (2008)
41. J. Santamaria, J. Garcia-Barriocanal, Z. Sefrioul, C. Leon, Int. J. Modern Phys. B **27**(19) (2013)
42. J. Salafranca, S. Okamoto, Phys. Rev. Lett. **105**, 256804 (2010)
43. G.A. Ovsyannikov, A.E. Sheyerman, A.V. Shadrin, Yu.V. Kislinskii, K.Y. Constantinian, A. Kalabykhov, JETP Lett. **97**, 145 (2013)
44. V.V. Demidov, I.V. Borisenko, A.A. Klimov, G.A. Ovsyannikov, A.M. Petrzhik, S.A. Nikitov, Zh Eksp, Teor. Fiz. **139**, 943 (2011)
45. G. Koster, L. Klein, W. Siemons et al., Rev. Mod. Phys. **84**, 253 (2012)
46. https://www.qdusa.com/products/mpms3.html
47. B.F. Woodfield, M.L. Wilson, J.M. Byers, Phys. Rev. Lett. **78**, 3201 (1997)
48. I. Asulin, O. Yuli, G. Koren, O. Millo, Phys. Rev. B **79**, 174524 (2009)
49. Yu.N. Khaydukov, G.A. Ovsyannikov, A.E. Sheyerman et al., Phys. Rev. B **90**, 035130 (2014)

50. A.E. Sheyerman, K.Y. Constantinian, G.A. Ovsyannikov, Yu.V. Kislinskii, A.V. Shadrin, A.V. Kalabukhov, Yu.N. Khaydukov, JETP **120**, 1024 (2015)
51. H.-U. Habermeier, G. Cristiani. Physica C **408–410**, 864 (2004)
52. P. Padhan, W. Prellier, R.C. Budhani, Appl. Phys. Lett. **88**, 192509 (2006)
53. M. Ziese, I. Vrejoiu, E. Pippel et al., Phys. Rev. Lett. **104**, 167203 (2010)
54. A.Y. Borisevich, A.R. Lupini, J. He et al., Phys. Rev. B **86**, 140102(R) (2012)
55. M. Ziese, F. Bern, A. Setzer et al., Eur. Phys. J. B **86**, 42 (2013)
56. V.N. Menshov, V.V. Tygyshev, JETP **125**, 136 (2004)
57. N.M. Kreines, FNT **28**, 807 (2002) [Low Temp. Phys. **28**, 581 (2002)]
58. N. Pugach, A.I. Buzdin, Appl. Phys. Lett. **101**, 242602 (2012)
59. P. Komissinskiy, G.A. Ovsyannikov, K.Y. Constantinian, Y.V. Kislinski, I.V. Borisenko, I.I. Soloviev, V.K. Kornev, E. Goldobin, D. Winkler, Phys. Rev. B **78**, 024501 (2008)
60. L. Mieville, D. Worledge, T.H. Geballe, R. Contreras, K. Char, Appl. Phys. Lett. **73**, 1736 (1998)
61. M. van Zalk, A. Brinkman, J. Aarts, H. Hilgenkamp, Phys. Rev. B **82**, 134513 (2010)
62. M.A. Khasawneh, T.S. Khaire, C. Klose, W.P. Pratt Jr., N.O. Birge, Supercond. Sci. Technol. **24**, 024005 (2011)
63. A.F. Volkov, K.B. Efetov, Phys. Rev. B **81**, 144522 (2010)
64. J.L. Cohn, J.J. Neumeier, C.P. Popoviciu, K.J. McClellan, Th. Leventouri, Phys. Rev. B **56**, R8495 (1997)
65. P. Kostic, Y. Okada, N.C. Collins, Z. Schlesinger J.W. Reiner, L. Klein, A. Kapitulnik, T.H. Geballe, M.R. Beasley, Phys. Rev. Lett. **81**, 2498 (1998)
66. A. Barone, J. Paterno, *Josephson Effect* (Physics and Application (Mir, Moscow, 1984)
67. A. Pal, Z.H. Barber, J.W.A. Robinson, M.G. Blamire, Nat. Commun. **5**, 3340–3344 (2014)
68. F.V. Komissinskiy, G.A. Ovsyannikov, Z.G. Ivanov, FTT **43**, 769 (2000)
69. Yu.V. Kislinkii, K.Y. Konstantinian, G.A. Ovsyannikov, F.V. Komissinskiy, I.V. Borisenko, A.V. Shadrin, JETP **106**, 800 (2008)
70. C. Klose, T.S. Khaire, Y. Wang, W.P. Pratt Jr., N.O. Birge, B.J. McMorran, T.P. Ginley, J.A. Borchers, B.J. Kirby, B.B. Maranville, J. Unguris, Phys. Rev. Lett. **108**, 127002 (2012)
71. G. Wild, C. Probst, A. Marx, R. Gross, Eur. Phys. J. B **78**, 509 (2010)
72. A.F. Volkov, K.B. Efetov, Phys. Rev. Lett. **102**, 077002 (2009)
73. A.I. Buzdin, A.S. Mel'nikov, N.G. Pugach, Phys. Rev. **B83**, 144515 (2011)